Journal of Magnetic Resonance Open 10–11 (2022) 100029

Contents lists available at ScienceDirect

Journal of Magnetic Resonance Open

journal homepage: www.sciencedirect.com/journal/journal-of-magnetic-resonance-open

Identification of potential short linear motifs (SLiMs) in intrinsically disordered sequences of proteins by fast time-scale backbone dynamics

Snigdha Maiti, Soumya De *

School of Bioscience, Indian Institute of Technology Kharagpur, Kharagpur, West Bengal 721302, India

ARTICLE INFO

Keywords:
Rigid segments
Order Parameter (S^2)
Solution NMR spectroscopy
Spectral density
Correlation times
Transcription Factors

ABSTRACT

Intrinsically disordered regions (IDRs) of proteins contain functionally important short linear motifs (SLiMs), which are composed of 3 to 10 residues. They are often crucial members in protein interaction networks (PINs) in various biological pathways. These short motifs are hard to identify and structurally characterize as very few techniques are amenable for studying IDRs. NMR spectroscopy has emerged as a powerful technique to study IDRs. Here we show that fast picosecond - nanosecond dynamics can be used to identify short rigid segments with significantly lower backbone flexibility compared to the rest of the IDR. Typically, the order parameter (S^2) for the backbone amide (NH) bond vector is used to measure residue-wise rigidity. We show that the parameter R_1R_2/(1-NOE) can be conveniently used to measure residue-wise rigidity for disordered regions. Both the parameters S^2 and R_1R_2/(1-NOE) identify the same rigid segments in the disordered region of the transcription factor SCR. Previously, we have shown that one of the identified rigid segments is indeed a SLiM and specifically interacts with a partner transcription factor. Furthermore, mutations were designed to introduce ionic interactions in a flexible linker connecting two rigid segments. Both the parameters S^2 and R_1R_2/(1-NOE) detect increased rigidity of this flexible linker in the mutants, which was not detected from backbone chemical shifts. Also, no change in global hydrodynamics properties were observed from size exclusion chromatography. Thus, backbone dynamics is highly sensitive to residue-wise rigidity in disordered sequences, which can be conveniently determined from R_1R_2/(1-NOE) and can identify potential functional SLiMs.

1. Introduction

An intrinsically disordered region (IDR) is a long stretch of amino acids in a polypeptide chain that does not fold into any three-dimensional structure under physiological conditions. Nearly 50% of the eukaryotic proteins have long disordered regions (>30 residues) [1,2]. In recent years, intrinsically disordered regions and proteins (IDRPs) have been shown to play important roles in several biological processes such as signaling pathways, transcription, translation, and cell cycle [3]. Mutations in IDRs have also been implicated in human diseases, such as neurodegeneration and cancer [4–6]. IDRPs mostly exert their function by binding to several partner molecules such as small molecules, DNA, RNA, or other proteins. Due to their ability to interact with multiple partner proteins, IDRPs are often found in the hubs in protein interaction networks [7].

Partner recognition by disordered regions in proteins is often mediated by short sequences known as motifs. Linear motifs in IDRPs are 3–10 residue long segments, which are involved in the formation of interaction interfaces [8]. They are also referred to as short linear motifs (SLiMs) or eukaryotic linear motifs (ELMs). SLiMs have two to four key residues that are important for function. Hence, even a point mutation in a disordered region can lead to a gain or loss of a linear motif. Most motifs are not conserved across species because of the high mutation rate in IDRs [9], which also hampers the identification of such motifs in IDRs by bioinformatics methods. Moreover, a lack of knowledge of the binding partner and weak interactions between IDRs and partner molecules make it difficult to experimentally identify these linear motifs. It is estimated that the eukaryotic proteome contains ~10^6 SLiMs and to date only 3600 motifs have been identified [10,11].

Recently, we have shown that potential SLiMs in IDRPs can be identified from the fast timescale (ps - ns) dynamics of the backbone measured by NMR spectroscopy [12]. In the transcription factors sex

; IDR, Intrinsically disordered region; SLiMs, Short linear motifs; IDRPs, Intrinsically disordered regions and proteins; SCR, Sex combs reduced; SSP, Secondary structure propensity; SEC, Size exclusion chromatography.

* Corresponding author at: School of Bioscience, Indian Institute of Technology Kharagpur, Kharagpur, West Bengal 721302, India.
E-mail address: somde@iitkgp.ac.in (S. De).

https://doi.org/10.1016/j.jmro.2021.100029

Available online 20 December 2021

combs reduced (SCR) and Deformed (DFD), we found that the disordered region consists of dynamically rigid segments (5 to 7 amino acids) connected by flexible linkers. One of the identified rigid segments specifically interacted with another transcription factor Extradentile, which is a known partner of SCR and DFD [13]. Hence, we proposed that the functionally important short linear motifs (SLiMs) can be identified in the IDRPs from their residue-wise rigidity, which is given by R_1R_2/(1-NOE).

In this work, we have investigated the effectiveness of the parameter R_1R_2/(1-NOE) in identifying rigid segments in disordered sequences as compared to the well-established order parameter (S^2), which is routinely used for identifying rigid and flexible amino acids in folded proteins. We found that both methods identify the same rigid and flexible segments in the disordered region in SCR. To further explore this, we studied SCR mutants whose flexible linker, connecting two rigid segments, were designed to be more rigid compared to the wildtype protein. The backbone atoms of the mutants were assigned and R_1, R_2, and $\{^1H\}-^{15}N$ NOE were measured. Indeed, the flexible linker is found to be more rigid in the mutants by both methods. Thus, the parameter R_1R_2/(1-NOE) provides a straightforward means to identify rigid and flexible segments in intrinsically disordered regions of proteins. Moreover, it is easier to identify the rigid and flexible regions from R_1R_2/(1-NOE) as its dynamic range (1.5 s^{-2} to 12 s^{-2}) for the residues in the disordered region is larger compared to the order parameter (0.15 to 0.6) for the same residues. Backbone chemical shifts also report on the secondary structure propensity (SSP) of each residue. Typically, higher SSP correlates with increased rigidity. However, for the wildtype and mutant SCR proteins, no regions with significantly increased SSP were observed. The hydrodynamic properties of the wildtype and mutant SCR proteins were investigated by analytical size exclusion chromatography (SEC) and no difference was observed. Overall, we show that backbone dynamics are highly sensitive to subtle differences in the residue-wise rigidity of disordered sequences and can be used to identify rigid segments and flexible linkers, which can be potential SLiMs and functionally important.

2. Materials and methods

2.1. Cloning, protein expression and purification

All SCR genes were cloned into the pET28a(+) expression vector that results in N-terminal His_6 tagged protein. The SCR^{WT} construct (residues K298 to K384) was generated by PCR and the sole cysteine Cys362 was mutated to serine by site-directed mutagenesis. The mutants SCR^{DM} (T317E and A320R) and SCR^{TM} (G314R, T317E, A320R) were generated using Q5® Site-Directed Mutagenesis protocol of NEB. Non-overlapping primers were designed for inverse PCR as described earlier [14] to simultaneously mutate the nearby residues T317 and A320 to generate SCR^{DM}. For the triple mutant SCR^{TM}, Gly314 was mutated to Arg-by inverse PCR using SCR^{DM} as a template. The PCR products were treated with DpnI enzyme to digest the methylated template DNA, followed by 5′ end phosphorylation using T4 polynucleotide kinase enzyme (Pnk) and ligation by T4 DNA ligase to generate the circular plasmids. The ligated products were transformed into *E. coli* DH5α competent cells. All the mutants were confirmed by DNA sequencing.

These proteins were expressed in *E. coli* BL21(λDE3) cells at 37 °C. For $^{15}N/^{13}C$ labeling, M9 minimal media supplemented with $^{15}NH_4Cl$ and ^{13}C-glucose, as the sole nitrogen and carbon source respectively, was used. The target proteins were purified using the Ni-NTA column that binds the His_6 tag. This affinity tag was removed from the purified proteins by Thrombin CleanCleave Kit from Sigma-Aldrich. Protein concentrations were determined by UV absorption using predicted molar absorptivity (ε280) [15]. For heteronuclear NMR experiments ^{15}N-labeled as well as ^{15}N-^{13}C double-labeled protein samples were used. The proteins were 0.2–0.6 mM with 7% D_2O for spinlock. For long-term stability of the proteins, 0.04% NaN_3 and 0.4 mM PMSF were also added to the final sample.

2.2. NMR experiments and backbone assignment

All NMR experiments were performed at 25 °C on ASCEND^{TM} 600 Bruker spectrometer equipped with a triple-resonance cryogenic probe head. SCR^{DM} was assigned as described elsewhere [12,14,16]. Briefly, double-labeled SCR^{DM} samples ($^{15}N/^{13}C$) were used for triple-resonance experiments such as HNCACB, CBCA(CO)NH, HNCO, HN(CA)CO, (H)CC(CO)NH-TOCSY and HNN [17]. The triple mutant SCR^{TM} was assigned using a ^{15}N-labelled sample where 3D- ^{15}N-TOCSY (mixing time- 60 ms) and 3D ^{15}N-NOESY (mixing time - 120 ms) experiments were used for identifying the amino acid type and sequential connection, respectively. All the spectra were processed and analyzed using NMRPipe [18] and Sparky [19], respectively.

A web tool termed as neighbor-corrected Structural Propensity Calculator (ncSPC, https://st-protein02.chem.au.dk/ncSPC) was used to calculate the secondary structure propensity of the disordered regions in SCR^{WT} and SCR^{DM}, using ncIDP library [20] as reference for random coil chemical shifts [21]. Experimentally determined chemical shifts of ^1H_N, $^{13}C_\alpha$, $^{13}C_\beta$, ^{13}CO and ^{15}N were used to calculate the secondary structure propensity (SSP) score where scores of 1.0 and −1.0 reflect fully formed α- or β-structure, respectively. The output was downloaded as an ASCII file and the SSP scores for each residue were plotted in excel.

Chemical shift perturbation of the backbone amide of each residue was calculated between two constructs of SCR using the following equation

$$\Delta\delta_{csp} = \sqrt{(\Delta\delta_H{}^2) + (0.154\Delta\delta_N)^2} \quad (1)$$

where, $\Delta\delta_H$ and $\Delta\delta_N$ are the observed shifts of a residue between the protein constructs in the proton and nitrogen dimension, respectively.

2.3. Backbone amide ^{15}N relaxation

Amide ^{15}N R_1, R_2 and steady-state heteronuclear $\{^1H\}-^{15}N$ NOE experiments were collected at 25 °C for all the proteins. Spectra for R_1 (50, 100, 150, 200, 400, 600, 900 and 1200 ms) and R_2 (50, 100, 150, 200, 250, 300, 400, and 500 ms) time series were collected in random order to minimize any systematic error. The recycle delay was set to 3 s between scans. Relaxation rate constants R_1 and R_2 were computed using in-house Matlab (MathWorks) codes by fitting the peak intensities (I) to single exponential decay

$$I = I_0 e^{(-tR_i)} \quad (2)$$

where I_0 is the Initial intensity, 'I' is the peak intensity, 't' is the relaxation delay, and R_i is either R_1 or R_2 [22,23]. Errors of the rate constants were assessed by Monte Carlo simulation. The heteronuclear $\{^1H\}-^{15}N$-NOE for every residue was calculated as a ratio of the peak heights obtained with and without 3 s of ^1H saturation. The recycle delay was set to 5 s. The spectral noise is used to assess the errors in $\{^1H\}-^{15}N$ NOE values by following the error propagation method.

2.4. Calculation of residue-wise rigidity from amide ^{15}N relaxation

The residue-wise rigidity of the disordered regions was measured from fast time scale (ps-ns) dynamics. The longitudinal (R_1), transverse (R_2) relaxation rate constants and heteronuclear $\{^1H\}-^{15}N$-NOE are calculated for each residue in the IDRs. The composite R_1R_2/(1-NOE) parameter gives a measure of rigidity for each residue [12]. Consecutive residues with a higher R_1R_2/(1-NOE) value than the average value of the disordered region constitute a rigid segment, whereas consecutive residues with a lower than average R_1R_2/(1-NOE) values constitute a flexible segment. Error for R_1R_2/(1-NOE) was calculated using propagation of error strategy

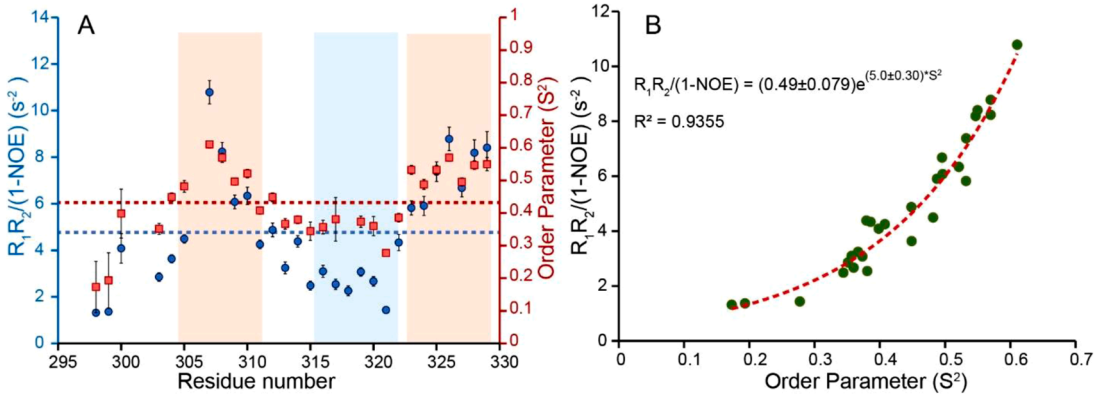

Fig. 1. **(A)** The order parameter (S^2) (red squares) and $R_1R_2/(1\text{-NOE})$ (blue circles) are plotted for each residue in the disordered region of SCR^{WT}. The average of S^2 and $R_1R_2/(1\text{-NOE})$ are shown as red and blue broken lines, respectively. The errors for $R_1R_2/(1\text{-NOE})$ were obtained using propagation of error method while the error in S^2 was calculated by Monte Carlo simulations. The rigid segments and flexible linkers are highlighted in red and blue, respectively. **(B)** Correlation plot of $R_1R_2/(1\text{-NOE})$ and order parameter (S^2) shows an increasing exponential dependence.

$$\text{Error} = \frac{R_1R_2}{1-\text{NOE}}\sqrt{\frac{\Delta R_1}{R_1}+\frac{\Delta R_2}{R_2}+\frac{\Delta\text{NOE}}{1-\text{NOE}}} \tag{3}$$

where, the errors of R_1, R_2, and NOE, are denoted as ΔR_1, ΔR_2 and ΔNOE, respectively.

2.5. Calculation of order parameter (S^2) and correlation times (τ_m, τ_e)

The order parameter (S^2) and correlation times (τ_m and τ_e) were determined as described by [24]. Spectral densities at five frequencies i.e. J(0), $J(\omega_N)$, $J(\omega_H - \omega_N)$, $J(\omega_H)$ and $J(\omega_H + \omega_N)$ were determined using the following expression

$$J(\omega) = \left(\frac{2}{5}\right)\left[S^2\frac{\tau_m}{1+(\omega\tau_m)^2} + (1-S^2)\frac{\tau_i}{1+(\omega\tau_i)^2}\right] \tag{4}$$

where,

$$1/\tau_i = 1/\tau_e + 1/\tau_m$$

Using these spectral densities, the ^{15}N-relaxation parameters were calculated as follows

$$R_1^{calc} = \left(\frac{d^2}{4}\right)(J(\omega_H-\omega_N)+3J(\omega_N)+6J(\omega_H+\omega_N))\Big/10^9 + c^2J(\omega_N)\Big/10^9 \tag{5}$$

$$R_2^{calc} = \left(\frac{d^2}{8}\right)(4J(0)+J(\omega_H-\omega_N)+3J(\omega_N)+6J(\omega_H)+6J(\omega_H+\omega_N))\Big/10^9 + \left(\frac{c^2}{6}\right)(3J(\omega_N)+4J(0))\Big/10^9 \tag{6}$$

$$NOE^{calc} = 1+\left(\frac{d^2}{4\times R_1}\right)\frac{\gamma_H}{\gamma_N}(6\times J(\omega_H+\omega_N) - J(\omega_H-\omega_N))\Big/10^9$$

$$d = \frac{\mu_0 h\gamma_H\gamma_N}{8\pi^2}\frac{1}{r_{NH}^3}$$

$$c = \frac{\omega_N}{\sqrt{3}}(\sigma_\parallel - \sigma_\perp)$$

$$r_{NH} = 1.02\ \text{Å}$$

$$\sigma_\parallel - \sigma_\perp = -160\ \text{ppm for backbone NH};\ -89.6\ \text{ppm for Trp residue NH} \tag{7}$$

The fitting parameters i.e. S^2, τ_m and τ_e for each residue in the disordered region were optimized by minimizing the target function

$$\chi^2 = \left(\frac{R_1^{exp}-R_1^{calc}}{\sigma R_1}\right)^2 + \left(\frac{R_2^{exp}-R_2^{calc}}{\sigma R_2}\right)^2 + \left(\frac{NOE^{exp}-NOE^{calc}}{\sigma NOE}\right)^2 \tag{8}$$

where the superscripts calc and exp denote calculated and experimental data, respectively, and σ is the experimental error. The errors in the fitted parameters (S^2, τ_m and τ_e) were estimated by Monte Carlo simulations. All calculations were performed by in-house Matlab codes.

2.6. Correlation between $R_1R_2/(1\text{-NOE})$ and order parameter (S^2)

The correlation between $R_1R_2/(1\text{-NOE})$ and order parameter (S^2) was fitted to an increasing exponential function as given below

$$\frac{R_1R_2}{(1-\text{NOE})} = Ae^{bS^2} \tag{9}$$

where, A and b are constants. The correlation plot was fitted to Eq. (9) using in-house Matlab code. The errors in A and b are determined using Monte-Carlo simulations. For error estimation, 50,000 synthetic datasets were generated by varying the experimental values of $R_1R_2/(1\text{-NOE})$ and S^2 within their experimental error using a normal distribution function. The error in A and b were determined as standard deviation of the 50,000 values generated from this simulation.

2.7. Analytical size exclusion chromatography (SEC)

Analytical SEC was performed to compare the oligomeric state and hydrodynamic shape of all three constructs SCR^{WT}, SCR^{DM}, and SCR^{TM} using a pre-packed Biorad ENrich^{TM} SEC 70 size exclusion column at 25 °C. The purified proteins were in a buffer containing 10 mM Tris (pH 8.2), 100 mM KCl and 1 mM EDTA.

3. Results

3.1. Comparison of the order parameter (S^2) and $R_1R_2/(1\text{-NOE})$ for the disordered region in wildtype SCR

Recently, we have shown that intrinsically disordered regions (IDRs) in proteins possess segments of residues (5 to 7 amino acids) with much lower backbone dynamics i.e. higher rigidity, compared to the rest of the IDRs, and are specifically involved in protein-protein interactions [12]. These segments were conveniently identified from a composite parameter $R_1R_2/(1\text{-NOE})$, where the longitudinal relaxation (R_1), transverse relaxation (R_2) and heteronuclear {^{1}H}–^{15}N NOE were measured by well-established ^{15}N backbone dynamics experiments [25]. The product $R_1R_2/(1\text{-NOE})$ gives a measure of rigidity for each residue. A segment of

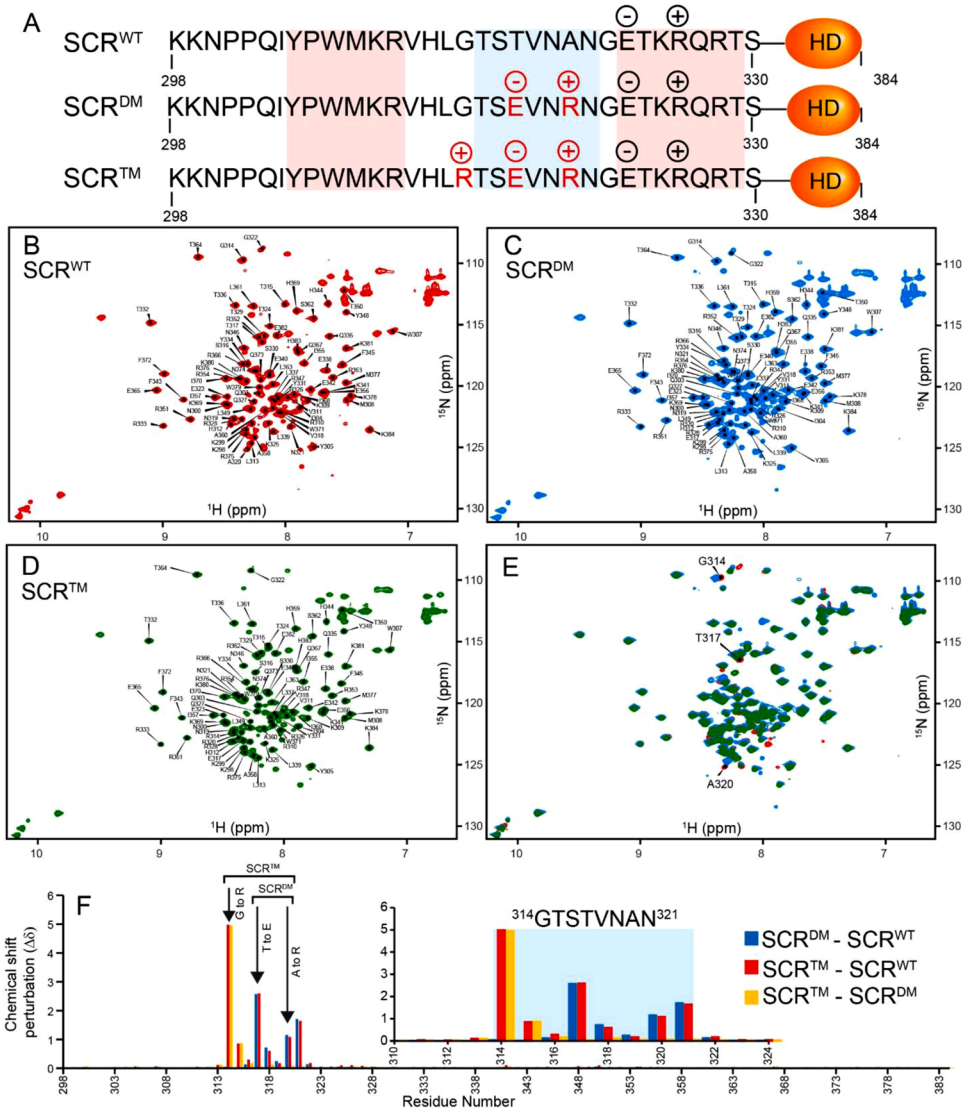

Fig. 2. (A) Schematic representation of the design of SCR mutants to enhance rigidity of the flexible linker. The folded DNA-binding homeodomain is colored orange and is labelled as HD. The N-terminal disordered part, attached to the folded homeodomain (HD), is denoted by its amino acid sequence (K298 to S330). The positions of the basic and acidic residues in the linker region are denoted by positive and negative signs, respectively. Wildtype residues are in black and mutated residues are in red. The rigid segments and flexible linkers, identified from SCR^{WT}, are highlighted in red and blue, respectively. The ^{1}H-^{15}N HSQC spectrum of **(B)** SCR^{WT}, **(C)** SCR^{DM}, **(D)** SCR^{TM} and **(E)** overlay of all three spectra are shown. Peaks corresponding to the mutated residues are labelled in panel E in the HSQC spectrum of SCR^{WT} to indicate peak shifts due to mutation. Peaks corresponding to the mutated residues are assigned but not shown for clarity. All the spectra were obtained at 25 °C using 600 MHz magnet. The protein concentrations were 0.5–0.8 mM in 20 mM phosphate buffer, pH 5.5. **(F)** Chemical shift perturbation from ^{1}H-^{15}N HSQC spectra is plotted as bars for all residues between SCR^{DM} and SCR^{WT} (blue), SCR^{TM} and SCR^{WT} (red), and SCR^{TM} and SCR^{DM} (yellow).

rigid residues can be identified as consecutive residues with R_1R_2/(1-NOE) values more than the average of the disordered region (Fig. 1A). This provides a straightforward analysis, based on well-established NMR relaxation methods, to identify rigid segments in IDRs of proteins.

For folded proteins, backbone amide ^{15}N dynamics is typically evaluated using the Lipari-Szabo method [26]. The measured backbone amide ^{15}N relaxation parameters R_1, R_2 and $\{^{1}H\}-^{15}N$ NOE are used to obtain the global correlation time (τ_m), and the residue-wise order parameter (S^2) and correlation time of the internal motion (τ_e) [27–30]. The global correlation time (τ_m) is determined from the ratio of R_2/R_1 of rigid residues identified based on $\{^{1}H\}-^{15}N$ NOE greater than 0.65 [31–33]. For disordered sequences in IDRPs, the correlation time (τ_m) is not global and varies for each residue. It has been shown that S^2, τ_m and τ_e can still be determined for each residue in disordered sequences from the NMR relaxation measurements [24].

The order parameter (S^2) provides an estimate of the motional restriction of each ^{15}N-^{1}H bond vector in proteins and has been shown to be related to conformational entropy of the bond vector [34,35]. To probe if the order parameter can reiterate the variation in flexibility in IDR and detect the aforementioned rigid and flexible segments, we have calculated the order parameter (S^2) for each residue in the IDR of wildtype SCR (SCR^{WT}). Indeed, the S^2 for each residue in the IDR showed variation in spatial restriction of the motional properties. Consecutive residues with moderately high and low values of S^2, corresponding to rigid and flexible segments respectively, can be identified from the plot (Fig. 1A). The variation in the parameters R_1R_2/(1-NOE) and S^2 followed the same pattern (Fig. 1A) and their correlation exhibits an increasing exponential dependence (Eq. (9)) with a correlation coefficient of 0.94 (Fig. 1B).

3.2. Design of rigidity enhancing mutations in the flexible region of SCR

Residues Thr315 to Asn321 constitute a flexible linker in the disordered region of SCR. In order to decrease the flexibility of this region, Thr317 and Ala320 were mutated to Glu-and Arg, respectively. These mutations resulted in alternate negative and positive charges at positions 317, 320, 323 and 326 (Fig. 2A). We reasoned that electrostatic attractions between positions i and $i + 3$ will restrict conformational sampling in the flexible linker and increase its rigidity. This double mutant is referred to as SCR^{DM}. Furthermore, Gly314 was mutated to Arg-and this triple mutant is referred to as SCR^{TM}.

^{1}H-^{15}N HSQC spectra of all the protein constructs have similar spectra indicating a properly folded DNA-binding homeodomain appended to disordered residues (Fig. 2B-D). The majority of the residues in SCR^{DM} and SCR^{TM} overlapped well with the wildtype construct

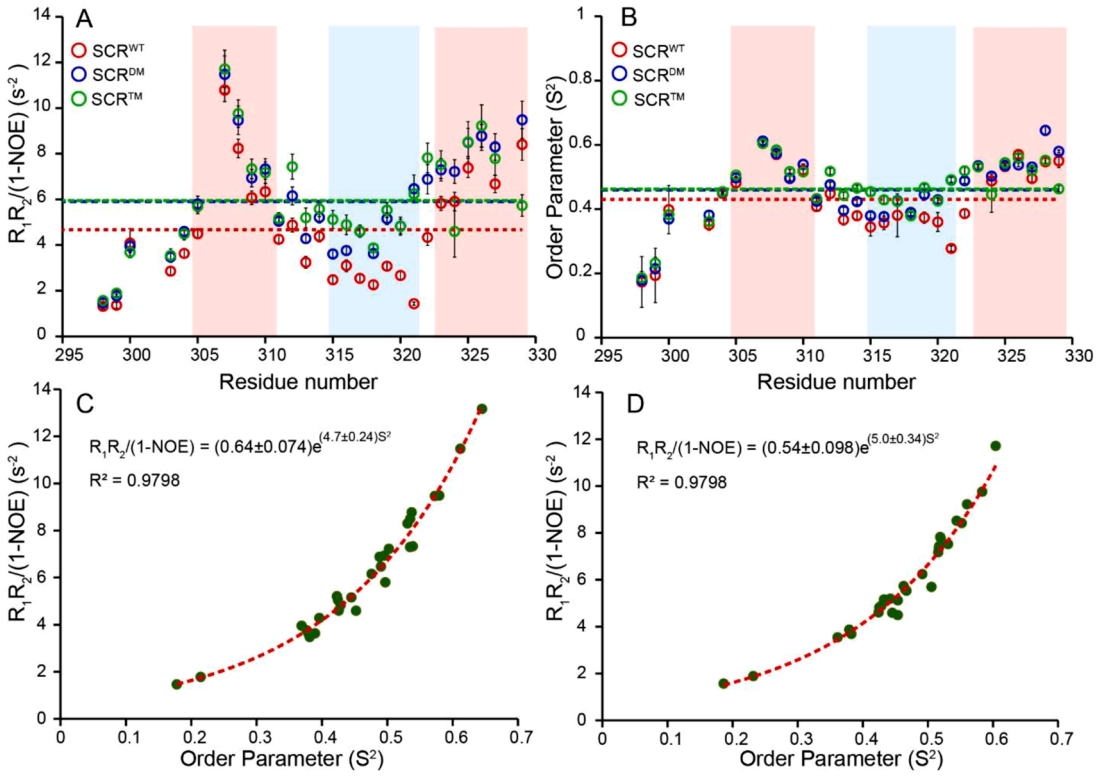

Fig. 3. **(A)** Residue-wise rigidity for SCR^{WT} (red circles), SCR^{DM} (blue circles) and SCR^{TM} (green circles) are plotted. **(B)** Order parameter (S^2) for each residue is plotted for SCR^{WT} (red circles), SCR^{DM} (blue circles) and SCR^{TM} (green circles). In both plots the rigid segments and flexible linker regions identified in SCR^{WT} are highlighted in red and blue, respectively. Also, in both plots the average values for each protein are shown as broken horizontal lines in same color as the corresponding data points. Correlation between the rigidity parameter ($R_1R_2/(1\text{-NOE})$) and the order parameter (S^2) are plotted for **(C)** SCR^{DM} and **(D)** SCR^{TM}. Both fit well to an increasing exponential function.

indicating no significant structural changes due to mutation (Fig. 2E). Mutations in the disordered region caused chemical shift perturbation for only a few neighboring residues of the mutation site (Fig. 2F).

3.3. Determination of residue-wise rigidity of SCR mutants

Backbone ^{15}N relaxation parameters (R_1, R_2 and $\{^1H\}-^{15}N$ NOE) were measured for both mutants SCR^{DM} and SCR^{TM}. The residue-wise rigidity $R_1R_2/(1\text{-NOE})$ for both were calculated and compared to the wildtype SCR^{WT} (Fig. 3A). As predicted, due to electrostatic interaction the flexible linker showed increased rigidity compared to the wildtype protein. The average rigidity of the linker region (Thr315 to Asn321) was 2.5 s^{-2} in SCR^{WT} which increased to 4.6 s^{-2} and 5.0 s^{-2} for SCR^{DM} and SCR^{TM}, respectively. The average rigidity of the first rigid segment (Tyr305 to Arg310) changes from 7.2 s^{-2} in SCR^{WT} to 8.2 s^{-2} in SCR^{DM} and 8.3 s^{-2} in SCR^{TM}. Similarly, the average rigidity of the second rigid segment (Glu323 to Thr329) are 7.2 s^{-2} in SCR^{WT}, 8.3 s^{-2} in SCR^{DM} and 7.2 s^{-2} in SCR^{TM}. Thus, the overall rigidity of the disordered region increased in both mutants with respect to the wildtype protein, and the major increment in rigidity occurred in the flexible linker where the

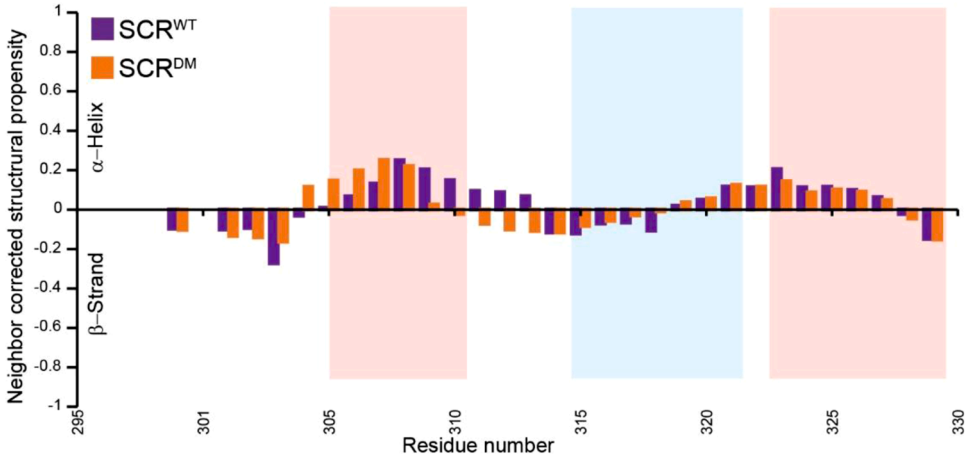

Fig. 4. Neighbor-corrected structural propensity (ncSPC) scores for SCR^{WT} (purple) and SCR^{DM} (orange) are plotted for the disordered residues. Positive and negative values correspond to propensities for α-helical and extended β-strand conformations, respectively. As a guide, the rigid segment and flexible linker regions, obtained from the backbone dynamic experiments of SCR^{WT}, are highlighted in red and blue, respectively.

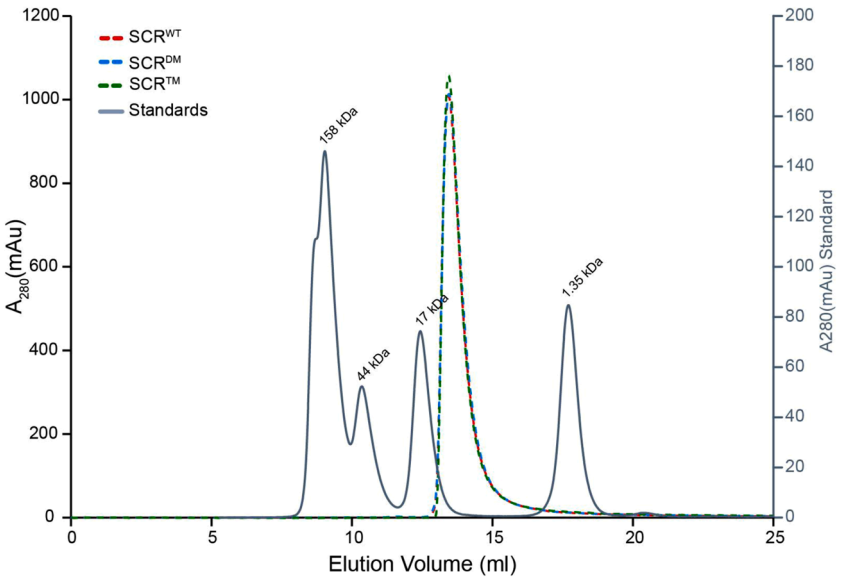

Fig. 5. Analytical size exclusion chromatography (SEC) elution profile of SCR^{WT} (red), SCR^{DM} (blue), and SCR^{TM} (green) shows single monodisperse peak for all the constructs. Overlay of elution profile shows that all the constructs elute at the same volume indicating similar hydrodynamic volume. The gray solid line in the profile indicates protein standards.

mutations were introduced.

Model-free analysis was also performed for the ^{15}N relaxation data of the two mutants to obtain the residue-wise order parameter (S^2) and correlation times (τ_m, τ_e). Similar to the residue-wise rigidity R_1R_2/(1-NOE), the order parameter follows the same pattern (Fig. 3B). The SCR^{WT} had an average S^2 value of 0.35 in the linker whereas for the same region the SCR^{DM} and SCR^{TM} showed an average S^2 value of 0.42 and 0.44, respectively. The average S^2 value of the first rigid segment is 0.54 for SCR^{WT} which remains unchanged for both SCR^{DM} and SCR^{TM}. The average S^2 value of the second rigid segment changes a little from 0.53 in SCR^{WT} to 0.55 in SCR^{DM} and 0.52 in SCR^{TM}. This indicates that the order parameter (S^2) for disordered regions is less sensitive to the subtle changes in residue-wise rigidity as compared to the rigidity parameter R_1R_2/(1-NOE). The exponential correlation between R_1R_2/(1-NOE) and S^2 values are 0.98 for both SCR^{DM} and SCR^{TM} (Fig. 3C-D).

3.4. Comparison of ensemble properties of SCR wildtype and mutant proteins

Unlike folded proteins, which have a unique three-dimensional structure, disordered sequences sample multiple conformations. Hence, an ensemble description of disordered sequences is more appropriate [36]. The backbone chemical shifts (^1H_N, ^{15}N, ^{13}CO, $^1H_\alpha$, $^{13}C_\alpha$, $^{13}C_\beta$) are sensitive to the local secondary structures and can be used to estimate the populations of α-helical and extended β-strand conformations for each amino acid in disordered sequences [37].

The secondary structure propensity (SSP) for each residue of SCR^{WT} and SCR^{DM} were obtained by comparing the experimentally measured chemical shifts of the backbone nuclei ^1H_N, $^{13}C_\alpha$, $^{13}C_\beta$, ^{13}CO and ^{15}N to the values expected for corresponding neighbor-corrected random coil chemical shifts for IDPs (ncIDP) using the online tool available at https://st-protein02.chem.au.dk/ncSPC. Positive SSP values close to +1 indicate α-helix and negative SSP values close to −1 indicate β-strand. The calculated propensities confirm that for both the SCR^{WT} and SCR^{DM} the region K298 to T329 is indeed disordered, with SSP scores in the − 0.2 to +0.2 range for the majority of the residues. Typically higher SSP score correlates with increased rigidity [38]. However, no rigid or flexible regions, with increased and decreased SSP, respectively, were observed in both SCR^{WT} and SCR^{DM} (Fig. 4).

Analytical size exclusion chromatography (SEC) can be used to estimate hydrodynamic dimensions of proteins [39]. For proteins with similar mass, separation in analytical SEC depends upon the hydrodynamic radii of these proteins. The hydrodynamic volume is a fundamental property of proteins that can provide an estimate of the proteins' overall shape i.e. whether it is compact, extended, or partially swollen. To probe if altered rigidity in the disordered region of SCR had any effect on the overall shape of the protein, the wildtype and the mutant SCR were characterized by analytical SEC. Interestingly, all the protein constructs have exactly the same elution volume (Fig. 5), which corresponds to monomeric mass of the proteins. The analytical SEC profile suggests that the wildtype SCR^{WT}, and the mutants SCR^{DM} and SCR^{TM} remain as monomers and have the same overall conformational shape. Thus, the structural effects of the mutations in the disordered region are limited to a few sequentially neighboring residues and do not affect the global structural properties of the protein.

4. Discussion

NMR spectroscopy is a powerful technique to explore dynamics of biomolecules at an atomic resolution and at different timescales. Innumerable biological functions rely on protein folding, ligand binding, catalysis and allostery. NMR spectroscopy provides a unique approach to study all these biological events occurring at different time scales ranging from picoseconds to hours [40,41]. Intrinsically disordered sequences, although lacking a folded structure, still experience motions at multiple timescales. They undergo librational motions in picoseconds; torsion angle dynamics, segmental and chain-like motions in nanoseconds; binding interactions in microseconds to milliseconds; and folding upon binding in millisecond or slower timescale [12,42–48] and NMR spectroscopy can be used to study all these dynamic events [49]. In this work, we have investigated the ability of fast picosecond - nanosecond dynamics to identify small rigid segments in intrinsically disordered regions (IDRs), which can lead to functionally important short linear motifs (SLiMs).

To explore the variation of residue-wise rigidity in IDRs, we have used two distinct methods of analyzing the backbone amide ^{15}N relaxation parameters. We used the Lipari-Szabo analysis to determine the generalized order parameter (S^2), which is routinely used for measuring residue-wise rigidity in folded proteins [14,16,50]. The other method uses the composite parameter R_1R_2/(1-NOE) to measure residue-wise

Table 1
Fitting results of simulated R_1R_2/(1-NOE) and S^2 to equation 9.

τ_e	τ_m	A	b	τ_e	τ_m	A	b	τ_e	τ_m	A	b	τ_e	τ_m	A	b
0.1	0.5	0.08	3.0	0.2	0.5	0.15	2.2	0.3	0.5	0.21	1.8	0.4	0.5	0.27	1.5
0.1	0.6	0.09	3.3	0.2	0.6	0.17	2.6	0.3	0.6	0.24	2.1	0.4	0.6	0.32	1.8
0.1	0.8	0.11	3.9	0.2	0.8	0.20	3.2	0.3	0.8	0.29	2.7	0.4	0.8	0.39	2.4
0.1	1	0.13	3.9	0.2	1	0.23	3.7	0.3	1	0.34	3.2	0.4	1	0.45	2.9
0.1	2	0.21	5.7	0.2	2	0.32	5.0	0.3	2	0.48	4.5	0.4	2	0.67	4.2
0.1	3	0.23	6.2	0.2	3	0.36	5.5	0.3	3	0.54	5.0	0.4	3	0.77	4.6
0.1	4	0.24	6.3	0.2	4	0.37	5.6	0.3	4	0.56	5.1	0.4	4	0.82	4.8
0.1	5	0.24	6.4	0.2	5	0.38	5.6	0.3	5	0.58	5.1	0.4	5	0.85	4.8

For a given set of τ_e and τ_m, and S^2 values ranging between 0.1 to 0.95, R_1, R_2 and $\{^1H\}-^{15}N$ NOE were calculated using Eqs. (5)-(7). The correlation plot of the composite parameter R_1R_2/(1-NOE) versus S^2 was fitted to Eq. (9) to obtain the parameters A and b. For the entire range of τ_m, τ_e and S^2 values (0.5 ns $\leq \tau_m \leq$ 5.0 ns; 0.1 ns $\leq \tau_e \leq$ 0.4 ns; 0.1 $\leq S^2 \leq$ 0.95), the correlation plot fitted well to Eq. (9).

rigidity [12]. Due to anisotropic motion of the disordered regions, the generalized order parameter S^2 as well as the global correlation time τ_m varies throughout the backbone. The variation in τ_m, assumption of an average bond length of N—H for all residues, and lack of clear separation of global (τ_m) and local motions (τ_e) add to the experimental errors in the relaxation measurements (R_1, and R_2 and $\{^1H\}-^{15}N$ NOE) and raises the uncertainty of the fitted S^2 values [24,31]. Moreover, the calculation of spectral densities at five frequencies followed by calculation of relaxation parameters is both computationally intensive and adds to the errors in the estimated S^2. On the other hand, the strength of the R_1R_2/(1-NOE) in identifying different segmental motions in IDR lies in its simplicity. Moreover, the dynamic range of the R_1R_2/(1-NOE) parameter is more than the order parameter. This is evident from the exponential dependence of the correlation of the two parameters. When rigidity increases, R_1R_2/(1-NOE) increases more rapidly compared to S^2, which makes it easier to identify the rigid segments.

The rigidity parameter R_1R_2/(1-NOE) is related to S^2 by an exponentially increasing function given by Eq. (9). To check the validity of this relationship, R_1, R_2, and $\{^1H\}-^{15}N$ NOE were calculated using the Eqs. (5)-7 for a range of τ_m, τ_e and S^2 values (0.5 ns $\leq \tau_m \leq$ 5.0 ns; 0.1 ns $\leq \tau_e \leq$ 0.4 ns; 0.1 $\leq S^2 \leq$ 0.95). For this entire range of values, the exponential relationship holds true between R_1R_2/(1-NOE) and S^2 (Table 1). However, the pre-exponential constant A and exponential constant b (Eq. (9)) varied with τ_m and τ_e. For a given value of τ_e, both A and b increased with increase in τ_m. Overall this simple relationship observed between R_1R_2/(1-NOE) and S^2 shows that for intrinsically disordered regions the parameter R_1R_2/(1-NOE) can be used as a measure of residue-wise rigidity, similar to the order parameter (S^2) for folded proteins.

It is important to note that the three parameters R_1, R_2 and $\{^1H\}-^{15}N$ NOE together provide a robust measure of residue-wise rigidity. Individually all three parameters have their own limitations. $\{^1H\}-^{15}N$ NOE is the most sensitive to fast time-scale motions, however it is magnetic field dependent. The longitudinal relaxation rate R_1 is the least sensitive among the three. It is dependent only on the fast time-scale motions (ps-ns) and independent of the slower time-scale motions (μs-ms). The transverse relaxation rate R_2, on the other hand, is sensitive to both fast and slow time-scale motions. Dynamics in slower time-scale manifests as chemical exchange (R_{ex}) and adds to the intrinsic transverse relaxation rate R_2. In disordered sequences, R_{ex} may result from protein aggregation [51–53] or residual secondary structures [46], which exchange between folded and unfolded conformations. The R_2 measurements may be performed at altered temperatures and with diluted samples if self-association is suspected. Hence, in order to identify rigid segments in intrinsically disordered regions it is important to identify the presence of R_{ex}. The product R_1R_2 is independent of anisotropic tumbling effect but increases significantly in the presence of chemical exchange [54]. Thus, comparison of residue-wise R_1R_2 with the average $\langle R_1R_2 \rangle$ over all residues in the disordered region readily identifies residues with significant R_{ex} and can be eliminated from further analysis. For instance, the disordered region ID3 in the CREB binding protein (CBP) has R_{ex} in its N-terminal region and can be readily identified (See supplemental figure S2, [55]). Interestingly, the C-terminal part of ID3, which lacks chemical exchange and hence enhanced R_2, binds to a novel partner ZFP106.

Generally, the functional binding interfaces in IDRs are short linear motifs (SLiMs) which are abundantly present in the eukaryotic proteome [56]. Although their abundance and importance in cellular functions are well appreciated, the identification and characterization of SLiMs by bioinformatics or experimental approach remain challenging due to their low sequence conservation and low binding affinity. Moreover, the molecular details of how flexible IDRs interact with other biomolecules is still a conundrum. A number of such motifs undergo disorder to order transition upon binding or show higher propensity to form transient secondary structures even in free form. Residual secondary structure or small hydrophobic clustering in disordered sequences can be identified via spin relaxation which shows local enhancement [46]. Therefore, it can be reasoned that SLiMs in IDRs often show reduced flexibility or restricted motions compared to other residues and they can be identified from fast time scale NMR relaxation studies [12,48]. The presence of rigid segments or preformed binding configuration in IDRs helps to attenuate the entropic penalty of binding with partner molecules. As SLiMs are mostly involved with partner protein interaction and sites for diverse post translational modification, their identification thorough NMR relaxation at atomic resolution allows to expedite the study of such interaction at molecular details.

5. Conclusions

The functionally important short linear motifs (SLiMs) can be identified in the disordered sequences of proteins from their residue specific motional properties such as residue-wise rigidity obtained from the composite parameter R_1R_2/(1-NOE) or estimation of generalised Order parameter (S^2). Segments of residues with higher rigidity may form functionally important SLiMs. Such dynamic analysis is determined in the free protein containing the disordered region and hence, is independent of the knowledge of the binding partner or interaction affinity between the protein and partner molecules. Rigid segments in IDRPs ensure that these stretches of amino acids sample a significantly smaller number of conformations, thus minimizing the loss in conformational entropy and increasing their binding affinity to partner molecules. Although, order parameter is helpful in identifying such segments, R_1R_2/(1-NOE) provides a straightforward parameter with better dynamic range to identify potential SLiMs.

Declaration of Competing Interest

The authors declare that they have no known competing financial interests or personal relationships that could have appeared to influence the work reported in this paper.

Acknowledgments

We are deeply indebted to Prof. Anil Kumar for his exceptional contributions to the field of NMR spectroscopy. His ground-breaking work in 2D NMR and nuclear Overhauser effect (NOE) essentially led to the expansion of solution NMR spectroscopy field for the determination of three-dimensional structures of biomolecules. We feel honored to dedicate this paper to him on the occasion of his 80th birthday.

The authors thank the Central Research Facility (CRF) at IIT Kharagpur for the use of NMR, and analytical size exclusion chromatography (SEC) facilities. This work has been supported by funding from the Science and Engineering Research Board (SERB), India (CRG/2020/004984). S.M acknowledges IIT Kharagpur for fellowship. The authors acknowledge Aditya J. Basak and Sagarika Dash for their help with analytical SEC data collection.

References

[1] Z. Peng, M.J. Mizianty, L. Kurgan, Genome-scale prediction of proteins with long intrinsically disordered regions, Proteins Struct. Funct. Bioinforma. 82 (2014) 145–158, https://doi.org/10.1002/prot.24348.

[2] A.K. Dunker, C.J. Brown, J.D. Lawson, L.M. Iakoucheva, Z. Obradović, Intrinsic disorder and protein function, Biochemistry 41 (2002) 6573–6582, https://doi.org/10.1021/bi012159+.

[3] P.E. Wright, H.J. Dyson, Intrinsically disordered proteins in cellular signalling and regulation, Nat. Rev. Mol. Cell Biol. 16 (2015) 18–29, https://doi.org/10.1038/nrm3920.

[4] V.N. Uversky, C.J. Oldfield, A.K. Dunker, Intrinsically disordered proteins in human diseases: introducing the D ^{2} concept, Annu. Rev. Biophys. 37 (2008) 215–246, https://doi.org/10.1146/annurev.biophys.37.032807.125924.

[5] R. van der Lee, M. Buljan, B. Lang, R.J. Weatheritt, G.W. Daughdrill, A.K. Dunker, M. Fuxreiter, J. Gough, J. Gsponer, D.T. Jones, P.M. Kim, R.W. Kriwacki, C. J. Oldfield, R.V. Pappu, P. Tompa, V.N. Uversky, P.E. Wright, M.M. Babu, Classification of intrinsically disordered regions and proteins, Chem. Rev. 114 (2014) 6589–6631, https://doi.org/10.1021/cr400525m.

[6] V. Vacic, P.R.L. Markwick, C.J. Oldfield, X. Zhao, C. Haynes, V.N. Uversky, L. M. Iakoucheva, Disease-associated mutations disrupt functionally important regions of intrinsic protein disorder, PLoS Comput. Biol. 8 (2012), https://doi.org/10.1371/journal.pcbi.1002709.

[7] C. Haynes, C.J. Oldfield, F. Ji, N. Klitgord, M.E. Cusick, P. Radivojac, V.N. Uversky, M. Vidal, L.M. Iakoucheva, Intrinsic disorder is a common feature of hub proteins from four eukaryotic interactomes, PLoS Comput. Biol. 2 (2006) 0890–0901, https://doi.org/10.1371/journal.pcbi.0020100.

[8] N.E. Davey, K. Van Roey, R.J. Weatheritt, G. Toedt, B. Uyar, B. Altenberg, A. Budd, F. Diella, H. Dinkel, T.J. Gibson, Attributes of short linear motifs, Mol. Biosyst. 8 (2012) 268–281, https://doi.org/10.1039/c1mb05231d.

[9] V. Neduva, R.B. Russell, Linear motifs: evolutionary interaction switches, FEBS Lett 579 (2005) 3342–3345, https://doi.org/10.1016/j.febslet.2005.04.005.

[10] K. Van Roey, B. Uyar, R.J. Weatheritt, H. Dinkel, M. Seiler, A. Budd, T.J. Gibson, N. E. Davey, Short linear motifs: ubiquitous and functionally diverse protein interaction modules directing cell regulation, Chem. Rev. 114 (2014) 6733–6778, https://doi.org/10.1021/cr400585q.

[11] P. Tompa, N.E. Davey, T.J. Gibson, M.M. Babu, A Million peptide motifs for the molecular biologist, Mol. Cell. 55 (2014) 161–169, https://doi.org/10.1016/j.molcel.2014.05.032.

[12] S. Maiti, B. Acharya, V.S. Boorla, B. Manna, A. Ghosh, S. De, Dynamic studies on intrinsically disordered regions of two paralogous transcription factors reveal rigid segments with important biological functions, J. Mol. Biol. 431 (2019) 1353–1369, https://doi.org/10.1016/j.jmb.2019.02.021.

[13] R. Joshi, L. Sun, R. Mann, Dissecting the functional specificities of two Hox proteins, Genes Dev 24 (2010) 1533–1545, https://doi.org/10.1101/gad.1936910.

[14] S. Boral, S. Maiti, A.J. Basak, W. Lee, S. De, Structural, dynamic, and functional characterization of a dnax mini-intein derived from spirulina platensis provides important insights into intein-mediated catalysis of protein splicing, Biochemistry 59 (2020) 4711–4724, https://doi.org/10.1021/acs.biochem.0c00828.

[15] E. Gasteiger, C. Hoogland, A. Gattiker, S. Duvaud, M.R. Wilkins, R.D. Appel, A. Bairoch, Protein identification and analysis tools on the ExPASy server, J.M. Walker (Ed.). Proteomics Protoc. Handb., Humana Press, Totowa, NJ, 2005, pp. 571–607, https://doi.org/10.1385/1-59259-890-0:571.

[16] A.J. Basak, S. Maiti, A. Hansda, D. Mahata, K. Duraivelan, S.V. Kundapura, W. Lee, G. Mukherjee, S. De, D. Samanta, Structural insights into N-terminal IgV domain of BTNL2, a T cell inhibitory molecule, suggests a non-canonical binding interface for its putative receptors, J. Mol. Biol. 432 (2020) 5938–5950, https://doi.org/10.1016/j.jmb.2020.09.013.

[17] M. Sattler, Heteronuclear multidimensional NMR experiments for the structure determination of proteins in solution employing pulsed field gradients, Prog. Nucl. Magn. Reson. Spectrosc. 34 (1999) 93–158, https://doi.org/10.1016/S0079-6565(98)00025-9.

[18] F. Delaglio, S. Grzesiek, G.W. Vuister, G. Zhu, J. Pfeifer, A. Bax, NMRPipe: a multidimensional spectral processing system based on UNIX pipes, J. Biomol. NMR. 6 (1995) 277–293, https://doi.org/10.1007/BF00197809.

[19] W. Lee, W.M. Westler, A. Bahrami, H.R. Eghbalnia, J.L. Markley, PINE-SPARKY: graphical interface for evaluating automated probabilistic peak assignments in protein NMR spectroscopy, Bioinformatics 25 (2009) 2085–2087, https://doi.org/10.1093/bioinformatics/btp345.

[20] K. Tamiola, B. Acar, F.A.A. Mulder, Sequence-specific random coil chemical shifts of intrinsically disordered proteins, J. Am. Chem. Soc. 132 (2010) 18000–18003, https://doi.org/10.1021/ja105656t.

[21] K. Tamiola, F.A.A. Mulder, Using NMR chemical shifts to calculate the propensity for structural order and disorder in proteins, Biochem. Soc. Trans. 40 (2012) 1014–1020, https://doi.org/10.1042/BST20120171.

[22] M.J. Stone, P.E. Wright, W.J. Fairbrother, A.G. Palmer, J. Reizer, M.H. Saier, Backbone dynamics of the bacillus subtilis glucose permease IIA domain determined from 15N NMR relaxation measurements, Biochemistry 31 (1992) 4394–4406, https://doi.org/10.1021/bi00133a003.

[23] M.J. Stone, K. Chandrasekhar, P.E. Wright, H.J. Dyson, A. Holmgren, Comparison of backbone and tryptophan side-chain dynamics of reduced and oxidized escherichia coli thioredoxin using 15N NMR relaxation measurements, Biochemistry 32 (1993) 426–435, https://doi.org/10.1021/bi00053a007.

[24] D. Yang, Y.K. Mok, J.D. Forman-Kay, N.A. Farrow, L.E. Kay, Contributions to protein entropy and heat capacity from bond vector motions measured by NMR spin relaxation, J. Mol. Biol. 272 (1997) 790–804, https://doi.org/10.1006/jmbi.1997.1285.

[25] N.H. Pawley, C. Wang, S. Koide, L.K. Nicholson, An improved method for distinguishing between anisotropic tumbling and chemical exchange in analysis of 15N relaxation parameters, J. Biomol. NMR. 20 (2001) 149–165, https://doi.org/10.1023/A:1011249816560.

[26] G. Lipari, A. Szabo, Model-free approach to the interpretation of nuclear magnetic resonance relaxation in macromolecules. 1. theory and range of validity, J. Am. Chem. Soc. 104 (1982) 4546–4559, https://doi.org/10.1021/ja00381a009.

[27] A.T. Alexandrescu, D. Shortlet, Backbone dynamics of a highly disordered 131 residue fragment of staphylococcal nuclease, J. Mol. Biol. 242 (1994) 527–546, https://doi.org/10.1006/jmbi.1994.1598.

[28] J.M. Schurr, H.P. Babcock, B.S. Fujimoto, A test of the model-free formulas. Effects of anisotropic rotational diffusion and dimerization, J. Magn. Reson. Ser. B. 105 (1994) 211–224, https://doi.org/10.1006/jmrb.1994.1127.

[29] G.M. Clore, P.C. Driscoll, A.M. Gronenborn, P.T. Wingfield, Analysis of the backbone dynamics of interleukin-1β using two-dimensional inverse detected heteronuclear15N-1H NMR spectroscopy, Biochemistry 29 (1990) 7387–7401, https://doi.org/10.1021/bi00484a006.

[30] A.M. Mandel, M. Akke, A.G. Palmer, Backbone dynamics of Escherichia coli ribonuclease HI: correlations with structure and function in an active enzyme, J. Mol. Biol. 246 (1995) 144–163, https://doi.org/10.1006/jmbi.1994.0073.

[31] L.E. Kay, D.A. Torchia, A. Bax, Backbone dynamics of proteins as studied by nitrogen-15 inverse detected heteronuclear NMR spectroscopy: application to staphylococcal nuclease, Biochemistry 28 (1989) 8972–8979, https://doi.org/10.1021/bi00449a003.

[32] P. Mercier, L. Spyracopoulos, B.D. Sykes, Structure, dynamics, and thermodynamics of the structural domain of troponin C in complex with the regulatory peptide 1-40 of troponin I, Biochemistry 40 (2001) 10063–10077, https://doi.org/10.1021/bi010748+.

[33] N.H. Pawley, J.D. Gans, L.K. Nicholson, Factors determining the reliable description of global tumbling parameters in solution NMR, J. Biomol. NMR. 24 (2002) 215–229, https://doi.org/10.1023/A:1021664605995.

[34] M. Akke, R. Briischweiler, A.G. Palmer, NMR Order Parameters and Free Energy: an Analytical Approach and Its Application to Cooperative Ca2+ Binding by Calbindin D9k, J Am Chem Soc 115 (1993) 9832–9833.

[35] D. Yang, L.E. Kay, Contributions to conformational entropy arising from bond vector fluctuations measured from NMR-derived order parameters: application to protein folding, J. Mol. Biol. 263 (1996) 369–382, https://doi.org/10.1006/jmbi.1996.0581.

[36] S. Kosol, S. Contreras-Martos, C. Cedeño, P. Tompa, Structural characterization of intrinsically disordered proteins by NMR spectroscopy, Molecules 18 (2013) 10802–10828, https://doi.org/10.3390/molecules180910802.

[37] J.A. Marsh, V.K. Singh, Z. Jia, J.D. Forman-Kay, Sensitivity of secondary structure propensities to sequence differences between α- and γ-synuclein: implications for fibrillation, Protein Sci 15 (2006) 2795–2804, https://doi.org/10.1110/ps.062465306.

[38] Y. Shen, A. Bax, Identification of helix capping and β-turn motifs from NMR chemical shifts, J. Biomol. NMR. 52 (2012) 211–232, https://doi.org/10.1007/s10858-012-9602-0.

[39] V.N. Uversky, Size-exclusion chromatography in structural analysis of intrinsically disordered proteins, 2012. 10.1007/978-1-4614-3704-8_11.

[40] A.G. Palmer, III, NMR probes of molecular dynamics: overview and comparison with other techniques, Annu. Rev. Biophys. Biomol. Struct. 30 (2001) 129–155, https://doi.org/10.1146/annurev.biophys.30.1.129.

[41] A. Sekhar, L.E. Kay, An NMR view of protein dynamics in health and disease, Annu. Rev. Biophys. 48 (2019) 297–319, https://doi.org/10.1146/annurev-biophys-052118-115647.

[42] S.N. Khan, C. Charlier, R. Augustyniak, N. Salvi, V. Déjean, G. Bodenhausen, O. Lequin, P. Pelupessy, F. Ferrage, Distribution of pico- and nanosecond motions in disordered proteins from nuclear spin relaxation, Biophys. J. 109 (2015) 988–999, https://doi.org/10.1016/j.bpj.2015.06.069.

[43] A. Abyzov, N. Salvi, R. Schneider, D. Maurin, R.W.H. Ruigrok, M.R. Jensen, M. Blackledge, Identification of dynamic modes in an intrinsically disordered protein using temperature-dependent NMR Relaxation, J. Am. Chem. Soc. 138 (2016) 6240–6251, https://doi.org/10.1021/jacs.6b02424.

[44] L. Mollica, L.M. Bessa, X. Hanoulle, M.R. Jensen, M. Blackledge, R. Schneider, Binding mechanisms of intrinsically disordered proteins: theory, simulation, and experiment, Front, Mol. Biosci. 3 (2016) 1–18, https://doi.org/10.3389/fmolb.2016.00052.
[45] C. Narayanan, K. Bafna, L.D. Roux, P.K. Agarwal, N. Doucet, Applications of NMR and computational methodologies to study protein dynamics, Arch. Biochem. Biophys. 628 (2017) 71–80, https://doi.org/10.1016/j.abb.2017.05.002.
[46] N. Salvi, A. Abyzov, M. Blackledge, Analytical description of NMR relaxation highlights correlated dynamics in intrinsically disordered proteins, Angew. Chemie - Int. Ed. 56 (2017) 14020–14024, https://doi.org/10.1002/anie.201706740.
[47] A.T. Look, A.T. Look, Oncogenic Transcription Factors in the Human Acute Leukemias, 1059 (2011). 10.1126/science.278.5340.1059.
[48] M. Schiavina, E. Salladini, M.G. Murrali, G. Tria, I.C. Felli, R. Pierattelli, S. Longhi, Ensemble description of the intrinsically disordered N-terminal domain of the Nipah virus P/V protein from combined NMR and SAXS, Sci. Rep. 10 (2020) 1–13, https://doi.org/10.1038/s41598-020-76522-3.
[49] N.V. Saibo, S. Maiti, B. Acharya, S. De, Analysis of structure and dynamics of intrinsically disordered regions in proteins using solution NMR methods, T. Tripathi, V.. Dubey (Eds.), Adv. Protein Mol. Struct. Biol. Methods (2021), https://doi.org/10.1016/B978-0-323-90264-9.00032-5.
[50] S.L. Chang, N. Tjandra, Temperature dependence of protein backbone motion from carbonyl 13C and amide 15N NMR relaxation, J. Magn. Reson. 174 (2005) 43–53, https://doi.org/10.1016/j.jmr.2005.01.008.
[51] R. Ahmed, J. Huang, M. Akimoto, T. Shi, G. Melacini, Atomic resolution map of hierarchical self-assembly for an amyloidogenic protein probed through thermal 15 N–R 2 correlation matrices, J. Am. Chem. Soc. 143 (2021) 4668–4679, https://doi.org/10.1021/jacs.0c13289.
[52] E.W. Martin, A.S. Holehouse, I. Peran, M. Farag, J.J. Incicco, A. Bremer, C.R. Grace, A. Soranno, R.V. Pappu, T. Mittag, Valence and patterning of aromatic residues determine the phase behavior of prion-like domains, Science 367 (80–) (2020) 694–699, https://doi.org/10.1126/science.aaw8653.
[53] S. Roy, S. Boral, S. Maiti, T. Kushwaha, A.J. Basak, W. Lee, A. Basak, S.L. Gholap, K. K. Inampudi, S. De, Structural and dynamic studies of the human RNA binding protein RBM3 reveals the molecular basis of its oligomerization and RNA recognition, FEBS J (2021) 1–18, https://doi.org/10.1111/febs.16301.
[54] J.M. Kneller, M. Lu, C. Bracken, An effective method for the discrimination of motional anisotropy and chemical exchange, J. Am. Chem. Soc. 124 (2002) 1852–1853, https://doi.org/10.1021/ja017461k.
[55] S. Contreras-Martos, A. Piai, S. Kosol, M. Varadi, A. Bekesi, P. Lebrun, A.N. Volkov, K. Gevaert, R. Pierattelli, I.C. Felli, P. Tompa, Linking functions: an additional role for an intrinsically disordered linker domain in the transcriptional coactivator, CBP, Sci. Rep. 7 (2017) 1–13, https://doi.org/10.1038/s41598-017-04611-x.
[56] M. Gouw, S. Michael, H. Sámano-Sánchez, M. Kumar, A. Zeke, B. Lang, B. Bely, L. B. Chemes, N.E. Davey, Z. Deng, F. Diella, C.-M. Gürth, A. Huber, S. Kleinsorg, L. S. Schlegel, N. Palopoli, K.V. Roey, B. Altenberg, A. Reményi, H. Dinkel, T. J. Gibson, The eukaryotic linear motif resource –2018 update, Nucleic Acids Res 46 (2018) D428–D434, https://doi.org/10.1093/nar/gkx1077.